

Gate Tunable Photovoltaic Effect in MoS₂ vertical P-N Homostructures

Simon A. Svatek^{1,2}, Elisa Antolin³, Der-Yuh Lin⁴, Riccardo Frisenda¹, Christoph Reuter⁵, Aday J. Molina-Mendoza², Manuel Muñoz⁶, Nicolás Agrait^{1,2}, Tsung-Shine Ko⁴, David Perez de Lara¹, Andres Castellanos-Gomez^{1*}*

¹ Instituto Madrileño de Estudios Avanzados en Nanociencia (IMDEA-Nanociencia), Faraday 9, Ciudad Universitaria de Cantoblanco, 28049, Madrid, Spain

² Departamento de Física de la Materia Condensada and Condensed Matter Physics Center (IFIMAC), Facultad de Ciencias, C/ Francisco Tomás y Valiente 7, Universidad Autónoma de Madrid, 28049, Madrid, Spain

³ Instituto de Energía Solar, Universidad Politécnica de Madrid, E.T.S.I. Telecomunicación, Ciudad Universitaria s/n Madrid, Madrid 28040, Spain

⁴ National Changhua University of Education, Bao-Shan Campus, No. 2, Shi-Da Rd, Changhua City 500, Taiwan, R.O.C

⁵ Department of Electrical Engineering and Information Technology, Technische Universität Ilmenau, Gustav-Kirchhoff-Str. 1, Ilmenau 98693, Germany

⁶ Instituto de Microelectrónica de Madrid (CNM, CSIC), C/ Isaac Newton 8, 28760 Tres Cantos, Madrid, Spain

*e-mail: simon.svatek@imdea.org and andres.castellanos@imdea.org

KEYWORDS: transition-metal dichalcogenides, photovoltaics, van der Waals assembly, p-type MoS₂

Abstract: P-n junctions based on vertically stacked single or few layer transition metal dichalcogenides (TMDCs) have attracted substantial scientific interest. Due to the propensity of TMDCs to show exclusively one type of conductivity, n- or p-type, heterojunctions of different materials are typically fabricated to produce diode-like current rectification and photovoltaic response. Recently, artificial, stable and substitutional doping of MoS₂ into n- and p-type has been demonstrated. MoS₂ is an interesting material to use for optoelectronic applications due to the potential of low-cost production in large quantities, strong light-matter interactions and chemical stability. Here we report the characterization of the optoelectronic properties of vertical homojunctions made by stacking few-layer flakes of MoS₂:Fe (n-type) and MoS₂:Nb (p-type). The junctions exhibit a peak external quantum efficiency of 4.7 %, a maximum open circuit voltage of 0.51 V, they are stable in air and their rectification characteristics and photovoltaic response are in excellent agreement to the Shockley diode model. The gate-tunability of the maximum output power, the ideality factor and the shunt resistance indicate that the dark current is dominated by trap-assisted recombination and that the photocurrent collection depends strongly on the spatial extent of the space charge region. We demonstrate a response time faster than 80 ms and highlight the potential to integrate such devices into quasi-transparent and flexible optoelectronics.

Introduction: Two-dimensional layered materials offer a broad variety of building blocks with remarkable electronic, photonic and mechanical properties.¹ In particular, TMDCs, such as WSe₂ and MoS₂, are considered promising candidates for photovoltaic devices due to their strong light-matter interactions²⁻⁴ and tunable (thickness-dependent) band gaps.^{5,6} There is a growing number of fundamental⁷⁻¹⁰ and applied¹¹⁻¹³ studies on thin layers of MoS₂. However, the formation of photovoltaic devices exclusively made of MoS₂ is hampered by the lack of samples with both transport characteristics, n-type and p-type, since MoS₂ typically exhibits only n-type doping. Previous experimental efforts to form junctions have therefore focused on layered heterojunctions formed by vertical van der Waals stacking of dissimilar materials, mostly in combination with WSe₂¹⁴⁻¹⁷, and less frequently with other compounds such as GaTe¹⁸, black phosphorus¹⁹, and graphene.^{20,21} Besides, the possibility to form homojunctions from MoS₂ has been explored with promising results but this could only be realised through superficial doping by exposing devices after processing to AuCl₃^{22,23}, through Schottky junctions²⁴, or through local electrostatic gating.²⁵⁻²⁸ Recently, stable p-type conduction by substitutional niobium doping has been demonstrated in MoS₂²⁹, which enables the formation of all-MoS₂ p-n junctions. Here we demonstrate that, fabricating MoS₂ homostructures from vertical van der Waals assembly of p-type MoS₂ (0.5% Nb doping, $\sim 3 \times 10^{19} \text{ cm}^{-3}$) and n-type MoS₂ (either 0.5% Fe doping, or native n-type material), we can create solar harvesting p-n junctions. By fitting the current-voltage characteristics of these junctions with the Shockley diode model at various gate voltages, we extract all diode parameters and analyse in detail their gate-dependence.

The underlying physical mechanisms of rectification and photovoltaic response in vertical TMDC heterojunctions are fundamentally different to the mechanisms governing conventional p-n junctions based on the concept of selective contacts. It has been proposed³⁰ and experimentally shown^{17,31} that in monolayer MoS₂/WS₂ heterojunctions the photovoltaic response and current-voltage characteristics are governed by interlayer tunnelling recombination of majority carriers and do not follow an exponential

law.¹⁷ The rectification is a result of the type-II band alignment with given band offsets for electrons and for holes. The maximum achievable photovoltage is limited by the smallest of these offsets, which in the case of MoS₂/WSe₂ is the band offset for electrons, approximately 0.7 eV.³⁰ Contrarily, in conventional p-n junctions selective contacts for electrons and holes are produced through p- and n-doping and the electrical characteristics are determined by drift and diffusion processes of minority carriers. The photovoltage is limited by the built-in field which in turn is limited by the material bandgap, which typically exceeds the band offsets in heterojunctions. In the case of bulk MoS₂ the direct band-gap is 1.8 eV and the indirect band-gap is 1.3 eV.⁶ This consideration is crucial when assessing the potential of TMDC-based devices for solar applications and it emphasizes the need to explore vertical devices comprising selective contacts produced by stable atomic doping of TMDCs. In this work we present the characterization of vertical MoS₂ p-n homojunctions in the intermediate thickness regime (15 - 19 nm) between the monolayer and the bulk. We demonstrate that the current-voltage characteristics are in excellent agreement with the Shockley diode model, implying that the carrier dynamics in our MoS₂ homojunctions is predominantly governed by drift and diffusion processes. Ideality factors around 2.5 indicate trap-assisted recombination in the depleted regions. The performance of the devices is substantially affected by the gate voltage (V_G) through the modulation of the carrier densities and the electric field at the junction. In particular, a positive effect of V_G on the open-circuit voltage (V_{OC}) is always accompanied by a negative effect on the short-circuit current (I_{sc}) which points to a carrier collection influenced by the spatial extent of the space charge region. Interestingly, not only the ideality factor and the reverse saturation current but also the parasitic shunt resistance is modulated by the gate, suggesting that tunnel-assisted recombination is still relevant in devices of moderate thickness (~ 15 nm).

Results and Discussion: The MoS₂:Nb and MoS₂:Fe single crystals were grown by the chemical vapour transport method described by Wang, S. Y. et al.³² and Suh, J. et al.²⁹ (For an exhaustive study of the material composition see reference 29). Thin flakes from about 10 to 10³ μm² in size were prepared by micromechanical exfoliation of bulk crystals and deposited onto a viscoelastic stamp (GelFilm by GelPak)³³. Upon optical inspection a flake was transferred onto an Au/Ti (40 nm/10 nm) metal lead on a 295 nm SiO₂/Si substrate by pressing the viscoelastic stamp onto the substrate and releasing it slowly. Figure 1a and b show schematically the fabrication steps along with optical images of the device. First, the n-type flake was deposited onto the substrate, partially overlapping with an Au/Ti (40 nm/10 nm) metal contact. Subsequently a p-type flake was transferred using the same method, overlapping with the first flake to form the vertical junction. The thicknesses of the flakes were determined to be 9 nm (MoS₂:Nb) and 6 nm (MoS₂:Fe) by atomic force microscopy.

We recorded the current density (J) as a function of the source drain voltage (V_{SD}) and the V_G . All measurements have been performed in ambient conditions. Figure 1c shows J - V_{SD} characteristics of the p-n (MoS₂:Nb – MoS₂:Fe) homojunction in the dark and under illumination with monochromatic light ($\lambda = 660$ nm, intensity 80 mW/cm²) at various V_G values. We observe rectifying J - V_{SD} characteristics in the dark and photovoltaic behaviour under illumination. The photoresponse characteristics are modulated by the Si-gate electrode by changing the charge carrier density. The generated electrical power density $P_{el} = J V_{SD}$ for various V_G is shown in Figure 1d. A maximum of $P_{el} = 0.42$ mW/cm² and $V_{OC} = 0.51$ V is

generated at $V_G = -30$ V. This exceeds reported V_{OCs} at similar intensities of van der Waals heterojunctions made of MoS₂/WSe₂^{9,17}, MoS₂/GaTe¹⁸, and MoS₂/black phosphorous¹⁹, although has been exceeded by graphene/MoS₂/WSe₂/graphene junction¹⁷ due to enhanced extraction. Each $J-V_{SD}$ trace in Figure 1c has been fitted independently using a circuital model. It comprises a Shockley-diode and parasitic resistances in series (R_S) and in parallel (R_P) and it is described by the equation: $J = J_0 \left(\exp \left(\frac{e(V_{SD} - JR_S)}{nkT} \right) - 1 \right) + \frac{V_{SD} - JR_S}{R_P} - J_L$, where k is the Boltzmann constant, e is the electron charge, T is the temperature, n is the ideality factor, J_0 is the reverse saturation current density of the diode and J_L is the photogenerated current density. The fits are overlaid in Figure 1c as solid lines, showing strong agreement between the experimental data and the Shockley model. The parameters n , J_0 , J_L , R_S , and R_P that optimize each fitting are collectively plotted in Figure 2, and behave as continuous functions of V_G .

The agreement between the data and the Shockley-diode model implies that the carrier dynamics can be explained by the presence of a built-in field $E_{built-in}$ and the associated space charge region and neutral regions. This is illustrated in an ideal band diagram, see Figure 1e, in which the space charge region is represented as the grey area. Note that only the junction area, highlighted with dotted lines in Figure 1b, is considered in the band diagram. In our devices, drift and diffusion of minority carriers exclusively takes place in the junction area and the space charge region does not spread horizontally beyond. This implies that none of the observed effects originates from parasitic Schottky junctions at the contacts (further discussion is provided below regarding Figure 6).

The presence of a gate voltage ($V_G \neq 0$ V) produces either depletion or accumulation in the carrier population of the flakes and causes an additional field E_{Gate} parallel to the built-in field $E_{built-in}$ at the junction (Figure 1f-g), which alters the band bending and the relative position of the bands with respect to the Fermi level. For negative V_G , the n-MoS₂ tends to be depleted, the p-MoS₂ accumulates carriers, and $E_{built-in}$ is reduced by E_{Gate} . This is accompanied by a reduction of the thickness of the space charge region since the density of ionized dopant atoms which provide the field is predetermined by the doping. A positive V_G has the opposite effects. Thus, the thickness of the space charge region grows with V_G . The band bending introduced by E_{Gate} resembles a forward source-drain bias for negative V_G and vice versa. In our device the p-MoS₂ is expected to be degenerate²⁹, which implies that the carrier accumulation or depletion takes place mostly in the n-MoS₂. This has been taken into account in Figure 1f-g, where the Fermi-level appears pinned to the valence band in the p-type region.

The modulation of the thickness of the space charge region by V_G affects the $J-V_{SD}$ characteristics plotted in Figure 1c and thereby the fitting parameters from the Shockley-diode model, which are presented in Figure 2. The Supplementary Information contains gate-dependent $J-V_{SD}$ characteristics in the dark (Figure S1). Ideality factor values in the range $n = [2 - 3.5]$ are indicative of recombination mechanisms that become less efficient as V_{SD} increases. Such recombination is associated with coupled defects and possibly tunnelling mechanisms^{34,35}, which most likely occur in the space charge region where defects are not saturated and where the electric field can enhance tunnelling processes. The dramatic increase of n with decreasing V_G in our devices is consistent with tunnelling-assisted recombination at traps in the space charge region since tunnelling becomes less effective as the total

field in the junction is reduced. It has to be noted that the depleted regions generated by V_G at the MoS₂/SiO₂ interface do not necessarily contribute to this recombination because carriers are prevented to approach the MoS₂/SiO₂ interface by the presence of the depleting fields. The amount of recombination, characterized by J_0 , increases with V_G and thus, with the thickness of the space charge region. The dark current, open-circuit voltage and power densities improve with decreasing V_G , mostly due to the increase of n and the decrease of J_0 .

The parameter J_L is the photogenerated current when no voltage is applied across the junction. Under those circumstances there can be no quasi-Fermi level split in the space charge region and therefore recombination can only take place in the rest of the device. Hence, J_L accounts for the total photogenerated electron-hole pairs reduced by the recombination that takes place in the volume which is not occupied by the space charge region under short-circuit conditions.³⁶ Consequently, J_L increases with V_G . The absolute value of J_L in our devices is in the range [1.9 – 3.0 mA/cm²].

Interestingly, the fittings yield different R_p values in the dark and under illumination. In the dark R_p shows a strong dependence on V_G . R_p quantifies local shuntings in the space charge region caused by tunnelling processes at coupled defects which is a known mechanism in conventional solar cells with high trap densities and $n > 2$.³⁵ As above, the tunnelling is enhanced when the total field is increased by V_G , which leads to a decrease in R_p . Under illumination we find a constant R_p independently of the gate. This is an apparent R_p related to a modulation of the photogenerated current and not to shunting. It reflects an increase of the photogenerated current as V_{SD} decreases which occurs due to the enlargement of the space charge region (similar to the case of positive V_G discussed above). This is known from other technologies of very thin solar cells, such as CdTe and chalcopyrite-based devices, in which the space charge region occupies a significant part of the total volume, and it is known as voltage dependent collection.³⁷

The series resistance R_s of the flakes depends on the occupation levels. As V_G increases the Fermi level is shifted towards the conduction band causing the resistance of the n-type (or p-type) flake to decrease (or increase). In the p-n junction we observe a decrease of the resistance with an increasing V_G which implies that the gate-dependence of the n-type flake is predominant. This can be attributed to degenerate doping of the p-flake, to the lower thickness of the n-type flake and a gate-screening effect, due to which the p-type flake is not effectively controlled by V_G since the n-type flake is screening the electric field. R_s shows the same gate-dependence in the dark and under illumination. When illuminated R_s is smaller than in the dark because of a higher over-all population. The values are in the range [60 - 100 MΩ] under illumination and [280 - 330 MΩ] in the dark.

Figure 1d shows that the positive effect of V_G on the photogenerated current is counteracted by the opposite effect on the photovoltage, causing P_{el} to increase as V_G decreases. The previous analysis allows us to attribute both effects to the modulation of the space charge region. This result differs fundamentally from the behaviour of heterojunction-based WSe₂/MoS₂ devices, where a variation in V_G affects directly the amount of interlayer recombination and leads to either an increase of photovoltage and photocurrent, or the reduction of both.¹⁷ Note that the device performance does not improve

indefinitely since V_G introduces non-linear effects in the series resistance of the flakes leading to the junction. Such behaviour is more pronounced in a MoS₂:Nb – native MoS₂ junction, see Supplementary Information, Figure S3.

Figure 3a and b show the dependence of the J - V_{SD} characteristics and P_{el} on the incident power with above-bandgap illumination ($\lambda = 660$ nm). The electrical power density reaches a maximum of 0.68 mW/cm². The maximum in short-circuit current is $J_{SC} = 3.3$ mA/cm² which corresponds to an external quantum efficiency of $EQE = 4.7$ % and a responsivity of 25 mA/W, which is similar to what has been achieved in vacuum in MoS₂ homojunctions made by surface doping (30 mA/W).²² A fill factor (FF) of 0.46 has been determined from $\max(P_{el}) = V_{OC} J_{SC} FF$. The dependences of V_{OC} (Figure 3c, left axis, blue squares) and J_{SC} (right axis, green circles) are, respectively, logarithmic and linear on the incident power which demonstrates that the J - V_{SD} characteristics are dominated by the Shockley-diode despite the presence of parasitic resistances. Besides, this confirms that the photocurrent is predominantly caused by the photovoltaic effect as opposed to thermoelectric effects.²⁸

By recording the photoresponse for various illumination wavelengths we characterize the junction further. Figure 4a shows J - V_{SD} characteristics for wavelengths between 405 nm and 1050 nm. The response has a peak in the vicinity of the exciton energies 659 nm and 611 nm (in monolayer material)³⁸, where the optical absorption is enhanced. For photons with higher wavelengths, $\lambda \geq 850$ nm, the device shows a negligible response, which is due to the reduced absorption of the indirect bandgap transitions. The response for wavelengths between 455 nm and 660 nm corresponds to $EQEs$ which range from 1.6 % to 4.5 %.

To determine the switching speed, we recorded the J against the time while the illumination ($\lambda = 660$ nm, intensity 80 mW/cm²) was alternately turned on and off (Figure 4b). When the device is unbiased (black curve) we extract an upper limit of 80 ms for both the rise and decay times, which are defined as the time required for J to rise (fall) to 90 % (10 %) of the difference between the initial and final value. Note, that this value is limited by our experimental setup. This temporal response is one order of magnitude faster than previously reported MoS₂ photodetectors with planar geometries³⁹, however, 9 orders of magnitude slower than values reported in graphene/TMD/graphene devices.⁴⁰ The strong differences in response times can be attributed to differences in the device geometries, carrier mobilities, flake thicknesses and extraction efficiencies. Response times in planar MoS₂ photodetectors are limited by the capacitance that is induced by trapped charge carriers. Faster response times in few-layer MoS₂ in ambient conditions (~10 ms) could to our knowledge only be realised by surface treatments, such as encapsulation with HfO₂⁴¹. Under forward bias, $V_{SD} = 0.5$ V (red curve), the photoresponse comprises also a photoconductance mechanism and the response time has been determined as 180 ms. We conclude that the photovoltaic effect in this geometry is at least 100 ms faster than other reported values. In line with results discussed earlier, our devices show a similar behaviour as conventional, selectively doped p-n junctions, in which the response time is dominated by diffusion mechanisms if operated in photovoltaic mode and a forward bias introduces a drift current which increases the response time.⁴²

We have also prepared a p-n (MoS₂:Nb – native MoS₂, 13 nm – 6 nm) homojunction and compared it to the p-n (MoS₂:Nb – MoS₂:Fe) above. We find the same qualitative dependences of n , I_0 , R_p , and R_s on the gate voltage. Under illumination with $\lambda = 660$ nm and an intensity of 80 mW/cm, the maximum power $P_{el} = 0.04$ mW/cm² is generated at $V_G = -10$ V and at $V_{SD} = 0.09$ V. We extract $V_{OC} = 0.14$ V and $FF = 0.4$. The $J_{SC} = 0.64$ mA/cm² corresponds to $EQE = 2.6$ % and a responsivity of 14 mA/W. We attribute the lower device performance to the lower doping level of the native MoS₂ in comparison to the intentionally doped MoS₂ (for additional data and a discussion of the doping levels, see Supporting Information).

The van der Waals assembly technique allows to easily form p-n junctions on virtually any substrate. Here, we explore the potential for transparent and flexible substrates. Figure 5a-d show optical micrographs of a p-n (MoS₂:Nb – MoS₂:Fe, 10 nm – 9 nm) homojunction on a polycarbonate substrate in reflection- and transmission-mode. We find that ~50 % of the incident white light is transmitted through the electrodes. The transmittance of the device area varies in the range of 70 ± 15 %, suggesting that our materials may be used in quasi-transparent applications. Figure 5e shows the J - V_{SD} characteristics in dark and under illumination of this flexible device. From circuit modelling we find $n = 2.46$, $I_0 = 0.3$ pA, $R_s = 0.7$ G Ω , and negligible R_p in the dark and $n = 2.84$, $I_0 = 5.8$ pA, $R_s = 70$ M Ω and $R_p = 7$ G Ω under illumination with $\lambda = 660$ nm at a power of 80 mW/cm². We extract the maximum power density $P_{el} = 0.11$ mW/cm² at $V_{SD} = 0.21$ V. The other figures of merit are $EQE = 1.5$ %, and responsivity of 8 mA/W for $J_{SC} = 0.66$ mA/cm², $V_{OC} = 0.32$ V, and $FF = 0.51$. After bending the substrate 50 times to a local radius of curvature of 2.5 cm (see Figure 5f) the J - V_{SD} characteristics remain unaltered. The lower device performance as compared to devices on SiO₂/Si substrates may be attributed to the absence of a reflective background.

To provide further evidence that the photocurrent is produced only in the junction area we fabricated another device (Figure 6b) and recorded scanning photocurrent maps with the set-up sketched in Figure 6a.^{43,44} The device is illuminated with a fiber-coupled LED ($\lambda = 505$ nm, spot diameter is 8 μ m) and moved with an xy-micrometer stage while simultaneously recording the intensity of the reflected light and the photocurrent. The spatial map of the reflected light intensity allows to determine the position of the focus⁴³. The photocurrent maps in Figure 6d and 6e were acquired in short-circuit and reverse bias conditions and reveal that the photovoltaic response exclusively occurs when the overlap region is illuminated. Under forward bias above V_{OC} , the resistance is determined by the resistance of the p-type flake which changes due to photoconductivity, see Figure 6f.

Summary: In summary, homojunctions based on few-layer MoS₂ have been fabricated and show external quantum efficiencies at 660 nm for different devices between 1.5 % and 4.6 %. We find that devices in this intermediate thickness regime (15 - 19 nm) between monolayers and bulk samples behave according to the Shockley-diode model. We have thoroughly analysed the gating effects on the photoresponse and conclude that the thickness of the space charge region decreases with the gate voltage which is correlated with an increase in device performance. We have demonstrated a gate-induced shifting of the maximum power point, J_{SC} and V_{OC} . The device shows fast response times compared with previous studies on MoS₂ layers, which indicates that a vertical design could pave the

way to faster MoS₂-based photodetectors. We have shown that devices made from substitutionally doped n-type material show superior device characteristics than devices made from native MoS₂. The p-n junctions demonstrate the potential of doped MoS₂ for quasi-transparent optical components in light harvesting cells and nanoscale optoelectronics.

SUPPORTING INFORMATION

Gate dependent $J-V_{SD}$ characteristics in the dark (S1). $J-V_{SD}$ characteristics at higher bias voltages (S2). Extend of the space charge region. Additional data regarding the MoS₂:Nb – native MoS₂ junction (S3). Comparison of gate dependence between junctions and single flakes (S4). Additional IV-curves of device in Figure 6 (S5).

AUTHOR CONTRIBUTIONS

SA Svatek has fabricated the devices and carried out the electrical characterisation. E Antolin generated the software that facilitates the electrical characterisation. DY Lin and TS Ko have fabricated the material. AJ Molina-Mendez and M Munoz have carried out the AFM characterisation. R Frisenda and C Reuter have carried out the photocurrent mapping. SA Svatek, E Antolin, N Agrait, D Perez de Lara, AC Castellanos-Gomez have analysed the data. AC Castellanos-Gomez has coordinated the project. All authors have edited the manuscript and contributed to discussions.

ACKNOWLEDGMENTS

S.A.S. and N.A. acknowledge funding by the European Commission through the FP7 ITN MOLESCO (Project Number 606728). E. A. gratefully acknowledges financial support from L'Oréal-UNESCO through the Women in Science program. A.J.M-M. acknowledges the financial support of MICINN (Spain) through the scholarship BES-2012-057346. D.Y. and T.S. acknowledge the support of the Ministry of Science and Technology of the Republic of China under the MOST 104-2112-M-018-004 and 104-2221-E-018-017. D. P. is thankful for funding from the Spanish Ministry of Economy and Competitiveness through FIS2015-67367-C2-1-P. R.F. thanks the Netherlands Organisation for Scientific Research (NWO) for the financial support through the research programme Rubicon with project number 680-50-1515. AC-G. acknowledges support from the BBVA Foundation through the fellowship "I Convocatoria de Ayudas Fundacion BBVA a Investigadores, Innovadores y Creadores Culturales" ("Semiconductores ultradelgados: hacia la optoelectronica flexible"), from the MINECO (Ramón y Cajal 2014 program, RYC-2014-01406), from the MICINN (MAT2014-58399-JIN) and from the Comunidad de Madrid (MAD2D-CM Program (S2013/MIT-3007)), and the European Commission under the Graphene Flagship, contract CNECTICT-604391.

REFERENCES

- 1 A. C. Ferrari, F. Bonaccorso, V. Fal'ko, K. S. Novoselov, S. Roche, P. Bøggild, S. Borini, F. H. L. Koppens, V. Palermo, N. Pugno, J. A. Garrido, R. Sordan, A. Bianco, L. Ballerini, M. Prato, E. Lidorikis, J. Kivioja, C. Marinelli, T. Ryhänen, A. Morpurgo, J. N. Coleman, V. Nicolosi, L. Colombo, A. Fert, M. Garcia-Hernandez, A. Bachtold, G. F. Schneider, F. Guinea, C. Dekker, M. Barbone, Z. Sun, C. Galiotis, A. N. Grigorenko, G. Konstantatos, A. Kis, M. Katsnelson, L. Vandersypen, A. Loiseau, V. Morandi, D. Neumaier, E. Treossi, V. Pellegrini, M. Polini, A. Tredicucci, G. M. Williams, B. Hee Hong, J.-H. Ahn, J. Min Kim, H. Zirath, B. J. van Wees, H. van der Zant, L. Occhipinti, A. Di Matteo, I. A. Kinloch, T. Seyller, E. Quesnel, X. Feng, K. Teo, N. Rupesinghe, P. Hakonen, S. R. T. Neil, Q. Tannock, T. Löfwander and J. Kinaret, *Nanoscale*, 2015, **7**, 4598–4810.
- 2 F. H. L. Koppens, T. Mueller, P. Avouris, A. C. Ferrari, M. S. Vitiello and M. Polini, *Nat. Nanotechnol.*, 2014, **9**, 780–793.
- 3 L. Britnell, R. V Gorbachev, R. Jalil, B. D. Belle, F. Schedin, A. Mishchenko, T. Georgiou, M. I. Katsnelson, L. Eaves, S. V Morozov, N. M. R. Peres, J. Leist, A. K. Geim, K. S. Novoselov and L. A. Ponomarenko, *Science*, 2012, **335**, 947–950.
- 4 E. Fortin and W. M. Sears, *J. Phys. Chem. Solids*, 1982, **43**, 881–884.
- 5 A. Splendiani, L. Sun, Y. Zhang, T. Li, J. Kim, C.-Y. Chim, G. Galli and F. Wang, *Nano Lett.*, 2010, **10**, 1271–1275.
- 6 K. F. Mak, C. Lee, J. Hone, J. Shan and T. F. Heinz, *Phys. Rev. Lett.*, 2010, **105**, 136805.
- 7 P. Tonndorf, R. Schmidt, P. Böttger, X. Zhang, J. Börner, A. Liebig, M. Albrecht, C. Kloc, O. Gordan, D. R. T. Zahn, S. Michaelis de Vasconcellos and R. Bratschitsch, *Opt. Express*, 2013, **21**, 4908.
- 8 H. J. Conley, B. Wang, J. I. Ziegler, R. F. Haglund, S. T. Pantelides and K. I. Bolotin, *Nano Lett.*, 2013, **13**, 3626–3630.
- 9 M. M. Furchi, D. K. Polyushkin, A. Pospischil and T. Mueller, *Nano Lett.*, 2014, **14**, 6165–6170.
- 10 O. V. Yazyev and A. Kis, *Mater. Today*, 2015, **18**, 20–30.
- 11 X. Cao, Y. Shi, W. Shi, X. Rui, Q. Yan, J. Kong and H. Zhang, *Small*, 2013, **9**, 3433–3438.
- 12 H. Li, G. Lu, Z. Yin, Q. He, H. Li, Q. Zhang and H. Zhang, *Small*, 2012, **8**, 682–686.
- 13 C. Zhu, Z. Zeng, H. Li, F. Li, C. Fan and H. Zhang, *J. Am. Chem. Soc.*, 2013, **135**, 5998–6001.
- 14 H. Heo, J. H. Sung, S. Cha, B.-G. Jang, J.-Y. Kim, G. Jin, D. Lee, J.-H. Ahn, M.-J. Lee, J. H. Shim, H. Choi and M.-H. Jo, *Nat. Commun.*, 2015, **6**, 7372.
- 15 Y. Gong, J. Lin, X. Wang, G. Shi, S. Lei, Z. Lin, X. Zou, G. Ye, R. Vajtai, B. I. Yakobson, H. Terrones, M. Terrones, B. K. Tay, J. Lou, S. T. Pantelides, Z. Liu, W. Zhou and P. M. Ajayan, *Nat. Mater.*, 2014, **13**, 1135–1142.
- 16 H. Fang, C. Battaglia, C. Carraro, S. Nemsak, B. Ozdol, J. S. Kang, H. A. Bechtel, S. B. Desai, F. Kronast, A. A. Unal, G. Conti, C. Conlon, G. K. Palsson, M. C. Martin, A. M. Minor, C. S. Fadley, E. Yablonovitch, R. Maboudian and A. Javey, *Proc. Natl. Acad. Sci.*, 2014, **111**, 6198–6202.
- 17 C. Lee, G. Lee, A. M. van der Zande, W. Chen, Y. Li, M. Han, X. Cui, G. Arefe, C. Nuckolls, T. F. Heinz, J. Guo, J. Hone and P. Kim, *Nat. Nanotechnol.*, 2014, **9**, 676–681.

- 18 F. Wang, Z. Wang, K. Xu, F. Wang, Q. Wang, Y. Huang, L. Yin and J. He, *Nano Lett.*, 2015, **15**, 7558–7566.
- 19 Y. Deng, Z. Luo, N. J. Conrad, H. Liu, Y. Gong, S. Najmaei, P. M. Ajayan, J. Lou, X. Xu and P. D. Ye, *ACS Nano*, 2014, **8**, 8292–8299.
- 20 L. Britnell, R. M. Ribeiro, A. Eckmann, R. Jalil, B. D. Belle, A. Mishchenko, Y.-J. Kim, R. V. Gorbachev, T. Georgiou, S. V. Morozov, A. N. Grigorenko, A. K. Geim, C. Casiraghi, A. H. C. Neto and K. S. Novoselov, *Science*, 2013, **340**, 1311–1314.
- 21 W. J. Yu, Y. Liu, H. Zhou, A. Yin, Z. Li, Y. Huang and X. Duan, *Nat. Nanotechnol.*, 2013, **8**, 952–958.
- 22 H.-M. Li, D. Lee, D. Qu, X. Liu, J. Ryu, A. Seabaugh and W. J. Yoo, *Nat. Commun.*, 2015, **6**, 6564.
- 23 M. S. Choi, D. Qu, D. Lee, X. Liu, K. Watanabe, T. Taniguchi and W. J. Yoo, *ACS Nano*, 2014, **8**, 9332–9340.
- 24 M. Fontana, T. Deppe, A. K. Boyd, M. Rinzan, A. Y. Liu, M. Paranjape and P. Barbara, *Sci. Rep.*, 2013, **3**.
- 25 J. S. Ross, P. Klement, A. M. Jones, N. J. Ghimire, J. Yan, D. G. Mandrus, T. Taniguchi, K. Watanabe, K. Kitamura, W. Yao, D. H. Cobden and X. Xu, *Nat. Nanotechnol.*, 2014, **9**, 268–272.
- 26 B. W. H. Baugher, H. O. H. Churchill, Y. Yang and P. Jarillo-Herrero, *Nat. Nanotechnol.*, 2014, **9**, 262–267.
- 27 A. Pospischil, M. M. Furchi and T. Mueller, *Nat. Nanotechnol.*, 2014, **9**, 257–261.
- 28 D. J. Groenendijk, M. Buscema, G. A. Steele, S. Michaelis de Vasconcellos, R. Bratschitsch, H. S. J. van der Zant and A. Castellanos-Gomez, *Nano Lett.*, 2014, **14**, 5846–5852.
- 29 J. Suh, T. Park, D.-Y. Lin, D. Fu, J. Park, H. J. Jung, Y. Chen, C. Ko, C. Jang, Y. Sun, R. Sinclair, J. Chang, S. Tongay and J. Wu, *Nano Lett.*, 2014, **14**, 6976–6982.
- 30 J. Kang, S. Tongay, J. Zhou, J. Li and J. Wu, *Appl. Phys. Lett.*, 2013, **102**, 12111.
- 31 M. M. Furchi, A. Pospischil, F. Libisch, J. Burgdörfer and T. Mueller, *Nano Lett.*, 2014, **14**, 4785–4791.
- 32 S. Y. Wang, T. S. Ko, C. C. Huang, D. Y. Lin and Y. S. Huang, *Jpn. J. Appl. Phys.*, 2014, **53**, 04EH07.
- 33 A. Castellanos-Gomez, M. Buscema, R. Molenaar, V. Singh, L. Janssen, H. S. J. van der Zant and G. A. Steele, *2D Mater.*, 2014, **1**, 11002.
- 34 A. Schenk and U. Krumbein, *J. Appl. Phys.*, 1995, **78**, 3185.
- 35 O. Breitenstein, J. Bauer, A. Lotnyk and J.-M. Wagner, *Superlattices Microstruct.*, 2009, **45**, 182–189.
- 36 A. Luque and S. Hegedus, *Handbook of Photovoltaic Science and Engineering*, John Wiley & Sons, Ltd, Chichester, UK, 2010.
- 37 S. Hegedus, D. Desai and C. Thompson, *Prog. Photovoltaics Res. Appl.*, 2007, **15**, 587–602.
- 38 S. Sim, J. Park, J. Song, C. In, Y. Lee, H. Kim and H. Choi, *Phys. Rev. B*, 2013, **88**, 75434.
- 39 O. Lopez-Sanchez, D. Lembke, M. Kayci, A. Radenovic and A. Kis, *Nat. Nanotechnol.*, 2013, **8**, 497–

- 501.
- 40 M. Massicotte, P. Schmidt, F. Violla, K. G. Schädler, A. Reserbat-Plantey, K. Watanabe, T. Taniguchi, K. J. Tielrooij and F. H. L. Koppens, *Nat. Nanotechnol.*, 2015, **11**, 42–46.
- 41 D. Kufer and G. Konstantatos, *Nano Lett.*, 2015, **15**, 7307–7313.
- 42 S. M. Sze, *Physics of Semiconductor Devices*, John Wiley & Sons, 1981.
- 43 M. Buscema, M. Barkelid, V. Zwiller, H. S. J. van der Zant, G. A. Steele and A. Castellanos-Gomez, *Nano Lett.*, 2013, **13**, 358–363.
- 44 C.-C. Wu, D. Jariwala, V. K. Sangwan, T. J. Marks, M. C. Hersam and L. J. Lauhon, *J. Phys. Chem. Lett.*, 2013, **4**, 2508–2513.

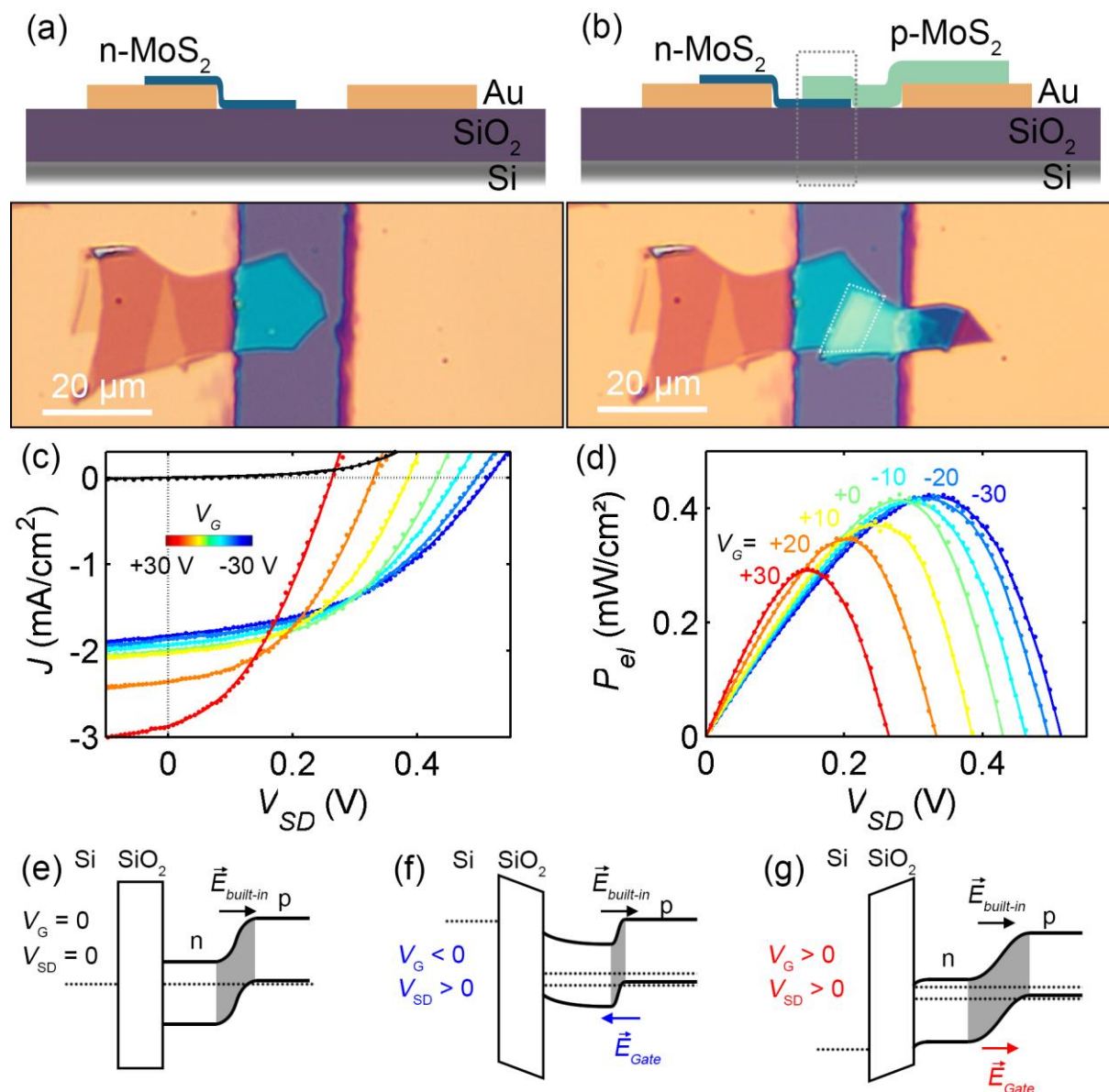


Figure 1. Device schematic and optical image of the n-type MoS₂ flake on top of Au/Ti lead before a) and after b) the transfer of p-type MoS₂. The dotted lines indicate the junction area. c) J - V_{SD} curves taken under illumination with $\lambda = 660$ nm at 80 mW/cm² at gate voltages from $+30$ V to -30 V in 10 V-steps (black: J - V_{SD} curve in the dark at $V_G = 0$ V). Experimental data is depicted as points and fits assuming the Shockley diode model are overlaid. d) The generated electrical power density P_{el} against V_{SD} at various V_G . (e-g) Band diagrams of the junction area at various values for V_G . The dotted lines represent the quasi Fermi levels for electrons and holes. The space charge region is highlighted in grey. V_G introduces an electric field E_{Gate} which enhances or reduces the total field and thereby contributes to the band bending.

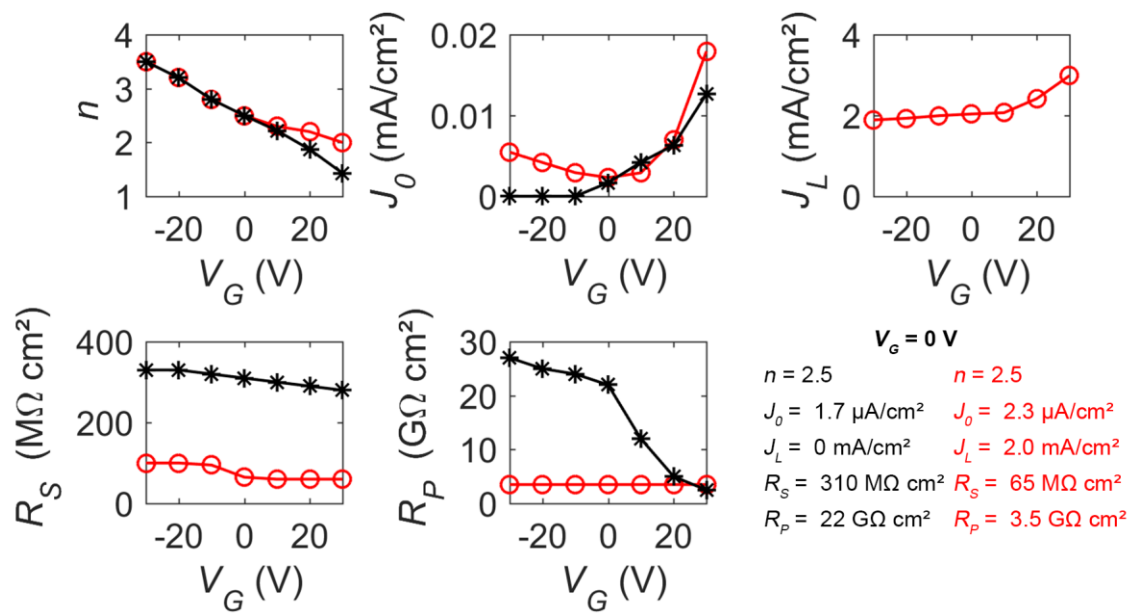


Figure 2. Fitting parameters extracted from Shockley-model-fits, see Figure 1 and S1. Red circles correspond to parameters under illumination ($\lambda = 660$ nm at 80 mW/cm²), black stars correspond to parameters in the dark.

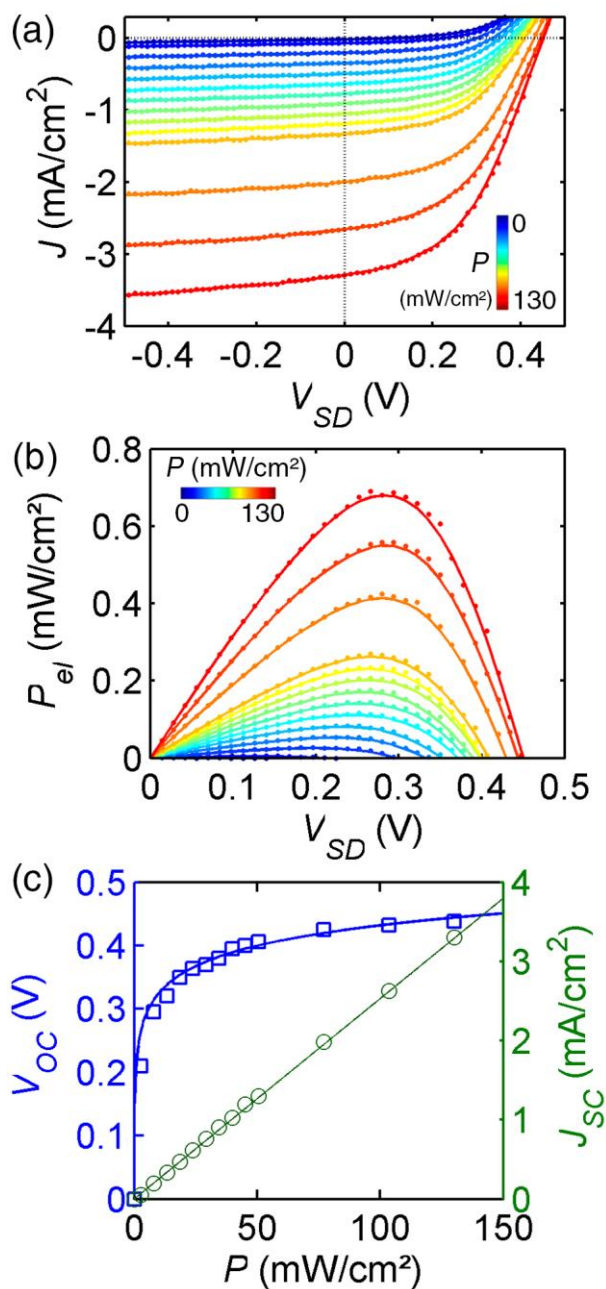


Figure 3. Device characteristics under illumination with $\lambda = 660$ nm at $V_G = 0$ V. The incident power ranges from 0 to 130 mW/cm². a) Power dependence of J - V_{SD} characteristics. b) Incident power dependence of the electrical power density P_{el} vs. V_{SD} . c) Logarithmic (linear) power-dependence of V_{OC} (J_{sc}) extracted from a).

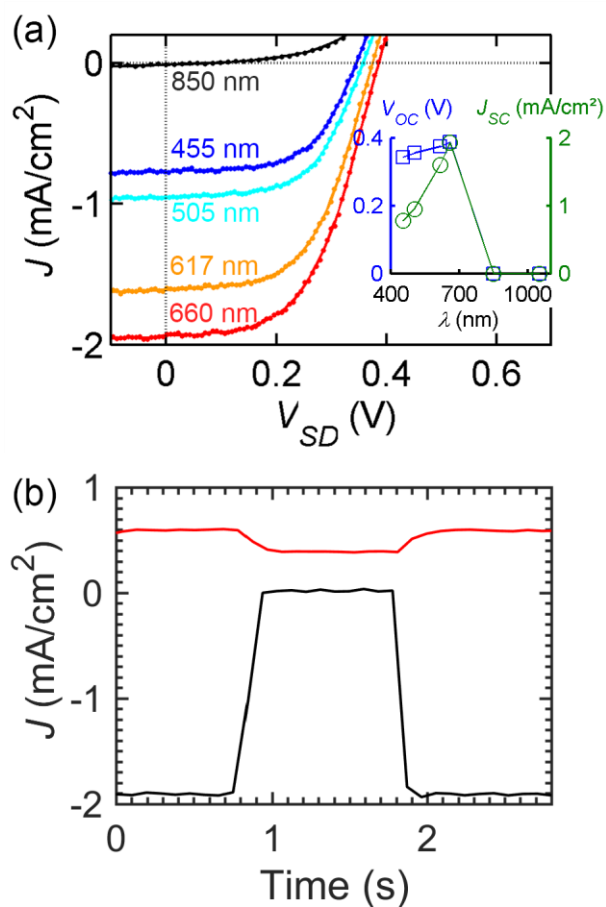


Figure 4. a) J - V_{SD} curves at different illumination wavelengths at 80 mW/cm². The device shows no photoresponse at wavelengths $\lambda \geq 850$ nm. The inset shows the dependence of V_{OC} and J_{SC} on the wavelength. b) Current density across the device against time at $V_G = 0$ V. The illumination (80 mW/cm at $\lambda = 660$ nm) was alternately turned on and off. Under short circuit conditions (black) we extract 80 ms as an upper limit for the response time. The response time at $V_{SD} = 0.5$ V (red) is determined as 180 ms.

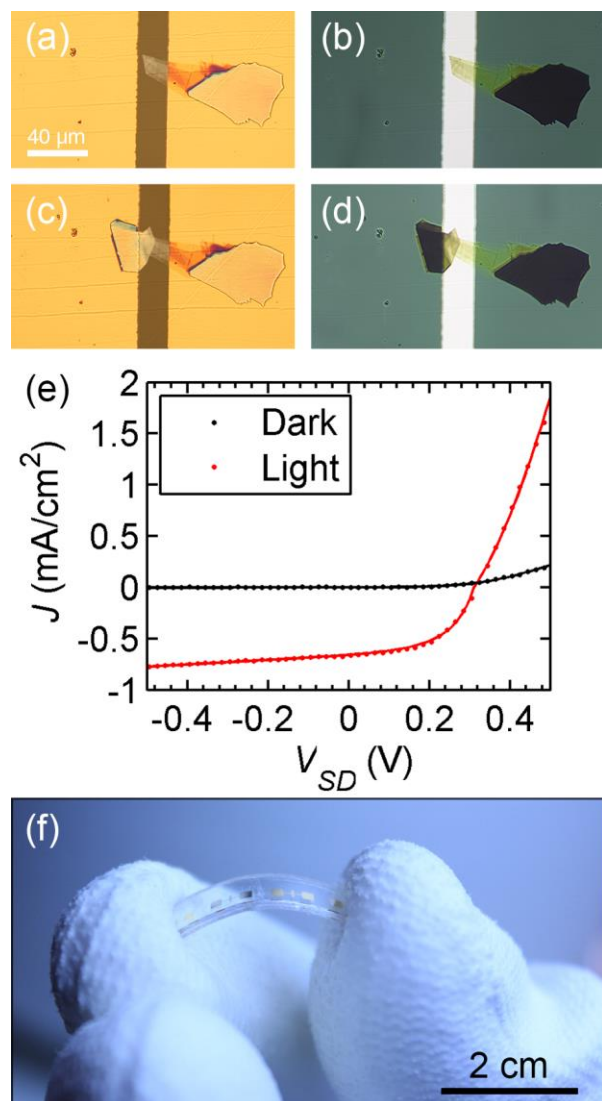


Figure 5. a)-d) Optical images of a quasi-transparent device with MoS₂:Nb (a, b) and the MoS₂:Nb - MoS₂:Fe junction (c, d) in bright field (a, c) and transmission-mode (b, d) on a polycarbonate substrate with Au/Ti (70 nm/15 nm) leads. e) J - V_{SD} curves in dark and under illumination with $\lambda = 660$ nm and 80 mW/cm². Fits assuming the Shockley diode model are overlaid as solid lines. f) A photograph of the device. The scale bar refers to the focal plane of the camera.

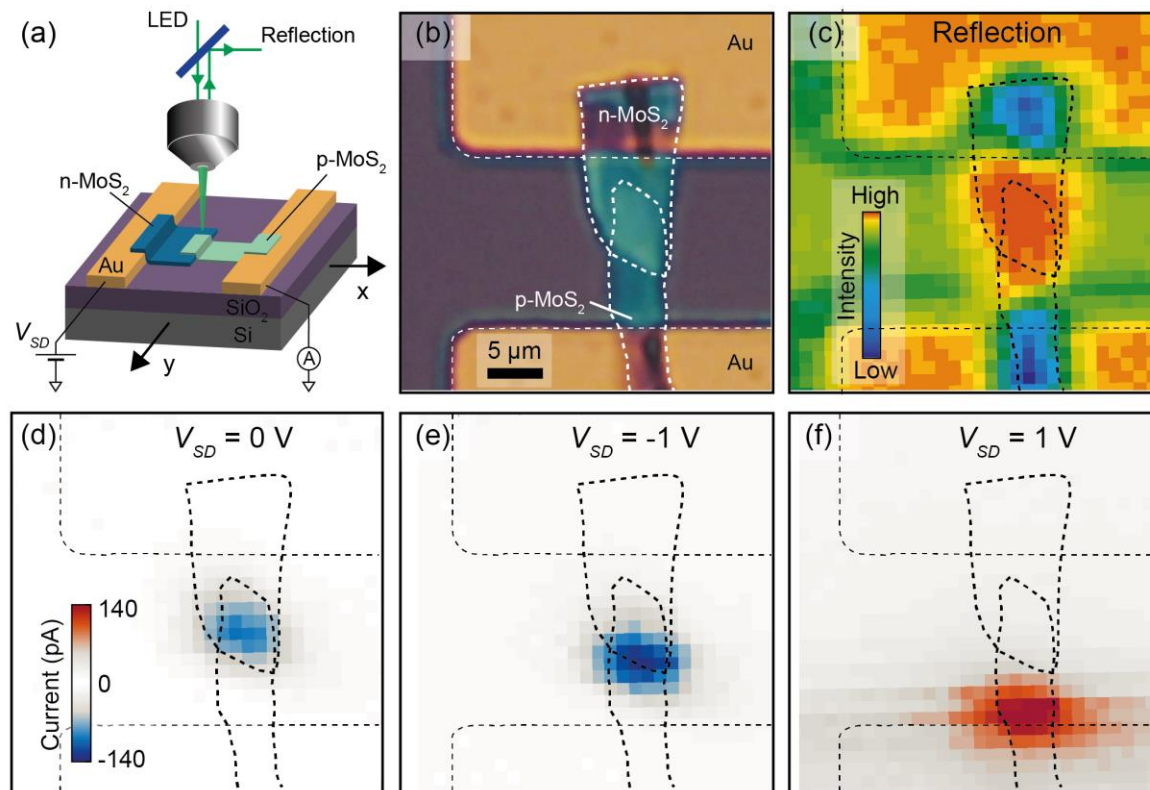


Figure 6. a) Sketch of the scanning photocurrent mapping set-up. A fibre-coupled LED ($\lambda = 505 \text{ nm}$, $P = 0.6 \mu\text{W}$) illuminates the sample which is moved using an xy-micrometer stage. A reflection map allows to determine the position of the focus. By applying V_{SD} , and measuring the photocurrent with respect to the stage position the spatial origin of the photocurrent can be determined. b) Optical image of the MoS₂ p-n homojunction. The dashed lines indicate the position of the electrodes and the two flakes. c) Spatial map of the reflection intensity. d-f) Photocurrent maps recorded at $V_{SD} = 0 \text{ V}$, $V_{SD} = -1 \text{ V}$ and $V_{SD} = 1 \text{ V}$. The photovoltaic response (in short-circuit and reverse bias conditions) originates in the overlap region. Under forward bias (above V_{oc}) the resistance of the device is determined by the resistance of the leads which change due to photoconductivity.

Supporting information

Gate Tunable Photovoltaic Effect in MoS₂ vertical P-N Homostructures

Simon A. Svatek^{1,2}, Elisa Antolin³, Der-Yuh Lin⁴, Riccardo Frisenda¹, Christoph Reuter⁵, Aday J. Molina-Mendoza², Manuel Muñoz⁶, Nicolás Agrait^{1,2}, Tsung-Shine Ko⁴, David Perez de Lara¹, Andres Castellanos-Gomez^{1*}*

¹ Instituto Madrileño de Estudios Avanzados en Nanociencia (IMDEA-Nanociencia), Faraday 9, Ciudad Universitaria de Cantoblanco, 28049, Madrid, Spain

² Departamento de Física de la Materia Condensada and Condensed Matter Physics Center (IFIMAC), Facultad de Ciencias, C/ Francisco Tomás y Valiente 7, Universidad Autónoma de Madrid, 28049, Madrid, Spain

³ Instituto de Energía Solar, Universidad Politécnica de Madrid, E.T.S.I. Telecomunicación, Ciudad Universitaria s/n Madrid, Madrid 28040, Spain

⁴ National Changhua University of Education, Bao-Shan Campus, No. 2, Shi-Da Rd, Changhua City 500, Taiwan, R.O.C

⁵ Department of Electrical Engineering and Information Technology, Technische Universität Ilmenau, Gustav-Kirchhoff-Str. 1, Ilmenau 98693, Germany

⁶ Instituto de Microelectrónica de Madrid (CNM, CSIC), C/ Isaac Newton 8, 28760 Tres Cantos, Madrid, Spain

*e-mail: simon.svatek@imdea.org and andres.castellanos@imdea.org

p-n junction (MoS₂:Nb – MoS₂:Fe): Gate dependent J - V_{SD} characteristics in the dark

The device shows gate-tunable rectification in the dark, see Figure S1. Since V_G acts similar to an effective bias voltage in respect to the modulation of the barrier height and the extent of the space charge region, the device is closer to breakdown at high V_G . The breakdown voltage is therefore reduced by a positive V_G . The Shockley model equations do not model the reverse breakdown which accounts for the deviation of the model from the data in reverse bias.

The inset shows the gate leakage-current for this particular device. The leakage current has been determined for all devices. Devices with leakage currents above 150 pA at $V_G = 30$ V or V_{SD} -dependent leakage were discarded.

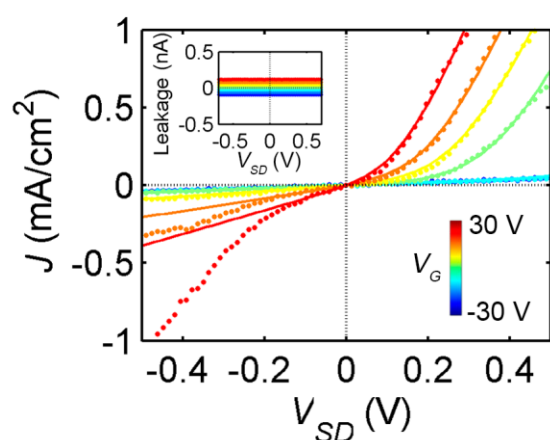


Figure S1. J - V_{SD} curves taken in the dark at V_G from +30 V to -30 V in 10-V steps. Experimental data is depicted as points and a Shockley-model-fit is overlaid. The inset shows the leakage-current to the gate electrode.

p-n junction (MoS₂:Nb – MoS₂:Fe): J - V_{SD} characteristics under illumination at high V_{SD}

Figure S2 shows J - V_{SD} curves at high V_{SD} . The current density J saturates at high positive bias V_{SD} . We attribute this to either Schottky barriers formed at the interface between the flakes and the metal leads or barriers forming in the direction parallel to the flake when moving away from the junction area toward the electrode contacting the MoS₂.¹ However, most relevant for photovoltaic applications is quadrant IV in which the effects of the leads are small, as discussed in the main text regarding Figure 3(c).

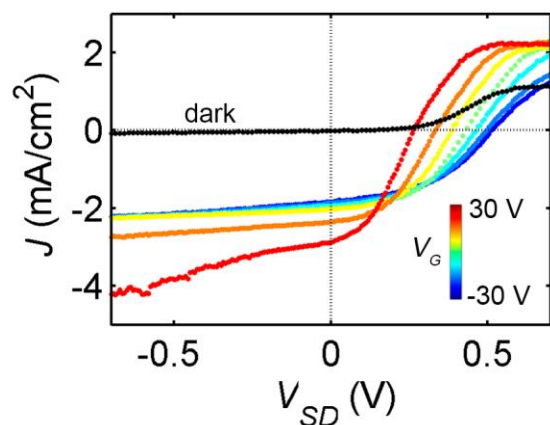


Figure S2. J - V_{SD} curves taken under illumination with 660 nm at 80 mW/cm² at gate voltages from +30 V to -30 V in 10-V steps (black: J - V_{SD} in the dark at $V_G = 0$ V).

The extent of the space charge region

In order to estimate the potential of substitutional Nb doping to generate ultra-thin MoS₂ homojunctions we can calculate the extent of the space charge region for the doping level achieved. The nominal doping level of the p-MoS₂ is 0.5% Nb. The actual concentration of dopant atoms has been estimated to be 0.4% from electron spectroscopy for chemical analysis (ESCA) measurements. The bulk electrical doping extracted from sheet resistance measurements is 3.0×10^{19} cm⁻³. Using the total depletion approximation² the thickness x_p of the p-side of the p-n junction under equilibrium is given by

$$x_p = \sqrt{\frac{2 \epsilon_{\text{MoS}_2} \epsilon_0 V_{\text{built-in}} N_D}{q N_A (N_A + N_D)}}$$

where ϵ_{MoS_2} is the relative permittivity of MoS₂ (11 from X. Chen et al.³), ϵ_0 is the permittivity of vacuum, q is the electron charge and N_A (N_D) is the acceptor (donor) density in the p (n) flake. $V_{\text{built-in}}$ is the built-in potential which can be calculated as $V_{\text{built-in}} = kT \ln(N_A N_D / n_i^2)$ where n_i is the intrinsic concentration (1.6×10^8 cm⁻³, from S. Kim et al.⁴). As a limit, assuming that $N_D = N_A$, we obtain $x_p = 5$ nm.

p-n junction (MoS₂:Nb – native MoS₂)

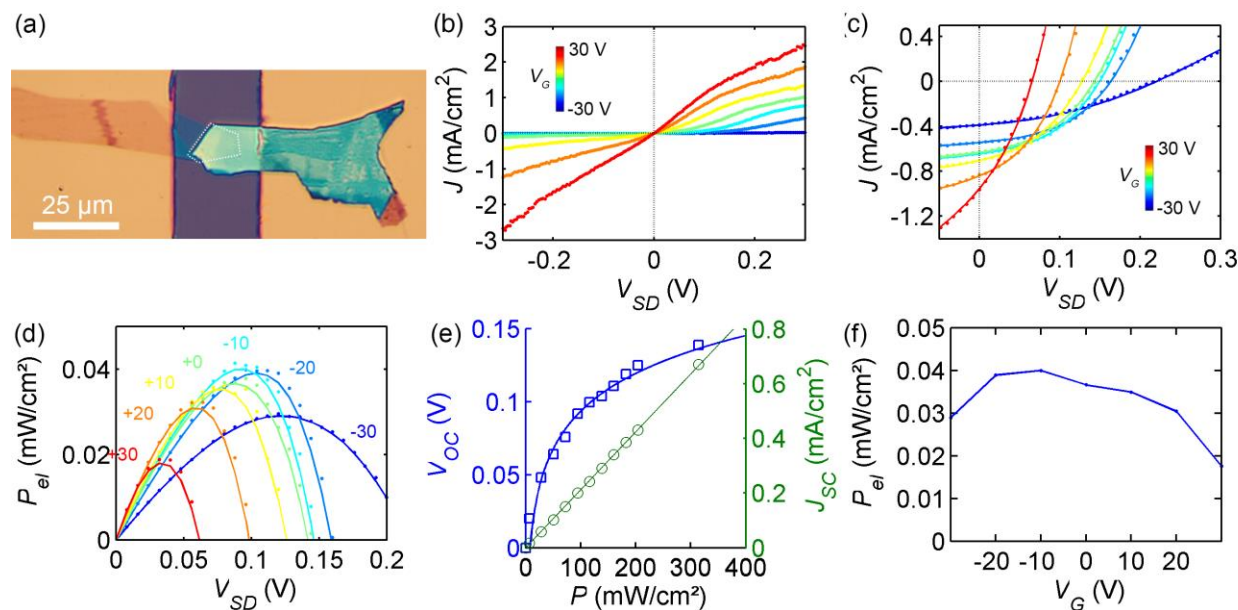


Figure S3. a) Optical image of the device. The dotted line indicates the junction area. b) J - V_{SD} curves taken in the dark and c) under illumination ($\lambda = 660$ nm, intensity 80 mW/cm²) with various V_G . Fits assuming a Shockley-diode are overlaid. d) Electrical power density P_{el} as a function of V_G . e) Logarithmic (and linear) power-dependence of V_{oc} (and I_{sc}) extracted from illumination power-dependent measurements. f) Gate-dependence of the electrical power P_{el} .

Gate dependence of dark current. Comparison to flakes

We have fabricated devices consisting of flakes of each of the three materials on 295 nm SiO₂/Si substrates with Au/Ti contacts. None of these devices exhibit a photovoltaic response. Therefore the photovoltaic response discussed in the main text originates indeed at the p-n junction and not at any other barrier, such as Schottky barriers at the contacts.

The gate dependences of the dark current in forward bias for single-flake devices are shown in figure S4. We find that the dark current across MoS₂:Nb decreases with V_G and it increases across the MoS₂:Fe and the native MoS₂ with V_G , confirming p- and n-doping. In our p-n junctions, we find the same qualitative gate dependence as in the n-type flakes. This indicates that the total conductance of the p-n junction is mostly influenced by the n-type flakes presumably due to their lower thickness.

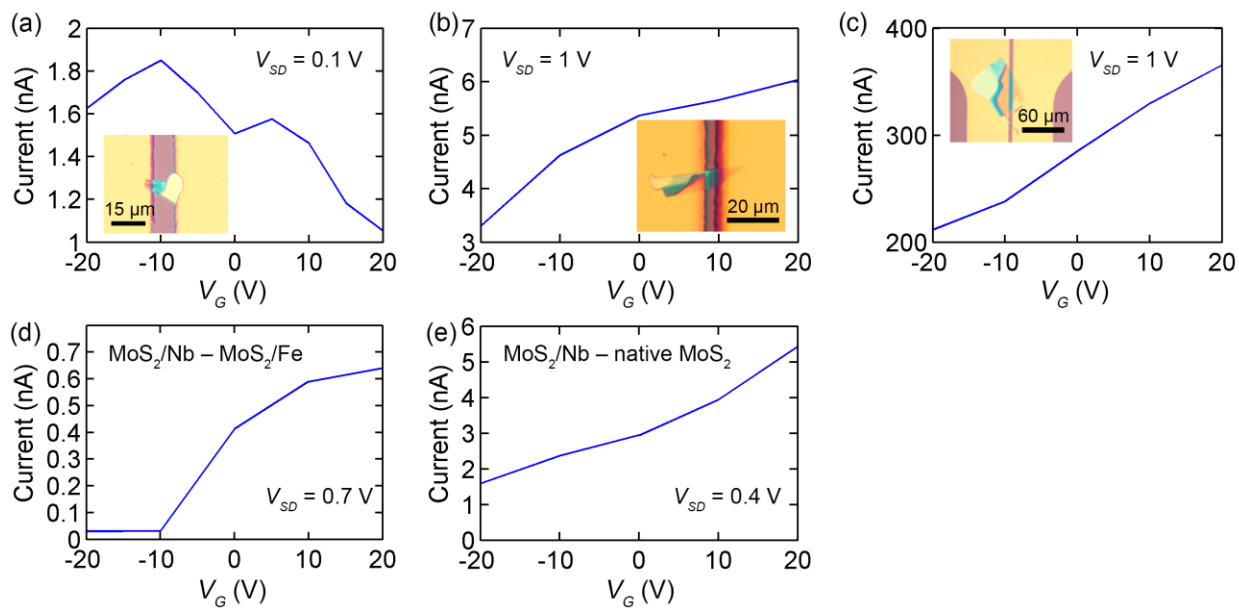


Figure S4. Gate dependence of dark current in forward bias conditions. a) MoS₂:Nb. b) MoS₂:Fe. c) Natural MoS₂. d) p-n junction, MoS₂:Nb.-MoS₂:Fe. e) p-n junction, MoS₂:Nb-natural MoS₂. The insets show optical images of the devices.

Additional IV-curve

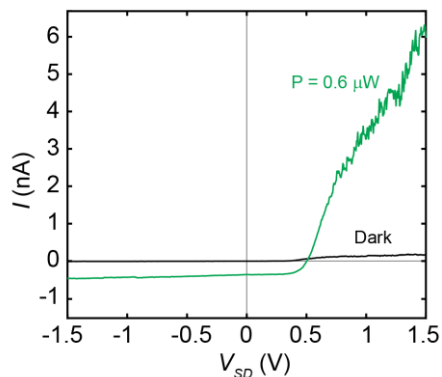


Figure S5. I - V_{SD} curves taken in the dark and under illumination ($\lambda = 530$ nm, intensity $6 \mu\text{W}$) of device in Figure 6.

SUPP. INFO. REFERENCES

- 1 M. Bernardi, M. Palumbo and J. C. Grossman, *Nano Lett.*, 2013, **13**, 3664–3670.
- 2 G. W. Neudeck, *The PN junction diode*, Addison-Wesley Longman, Incorporated, Volume 2 o., 1983.
- 3 X. Chen, Z. Wu, S. Xu, L. Wang, R. Huang, Y. Han, W. Ye, W. Xiong, T. Han, G. Long, Y. Wang, Y. He, Y. Cai, P. Sheng and N. Wang, *Nat. Commun.*, 2015, **6**, 6088.
- 4 S. Kim, A. Konar, W.-S. Hwang, J. H. Lee, J. Lee, J. Yang, C. Jung, H. Kim, J.-B. Yoo, J.-Y. Choi, Y. W. Jin, S. Y. Lee, D. Jena, W. Choi and K. Kim, *Nat. Commun.*, 2012, **3**, 1011.